The Astrophysical Journal, 769:28 (10pp), 2013 May 20 doi:10.1088/0004-637X/769/1/28
© 2013. The American Astronomical Society. All rights reserved. Printed in the U.S.A.

INFLATION OF A DIPOLE FIELD IN LABORATORY EXPERIMENTS: TOWARD AN UNDERSTANDING OF MAGNETODISK FORMATION IN THE MAGNETOSPHERE OF A HOT JUPITER

V. M. Antonov[1], E. L. Boyarinsev[1], A. A. Boyko[1], Yu. P. Zakharov[1], A. V. Melekhov[1], A. G. Ponomarenko[1], V. G. Posukh[1], I. F. Shaikhislamov[1], M. L. Khodachenko[2,3], and H. Lammer[2]
[1] Institute of Laser Physics SB RAS, Novosibirsk, Russia
[2] Space Research Institute, Austrian Acad. Sci., Graz, Austria; maxim.khodachenko@oeaw.ac.at
[3] Skobeltsyn Institute of Nuclear Physics, Moscow State University, Moscow, Russia
Received 2012 June 15; accepted 2013 April 2; published 2013 May 2

ABSTRACT

Giant exoplanets at close orbits, or so-called hot Jupiters, are supposed to have an intensive escape of upper atmospheric material heated and ionized by the radiation of a host star. An interaction between outflowing atmospheric plasma and the intrinsic planetary magnetic dipole field leads to the formation of a crucial feature of a hot Jupiter's magnetosphere—an equatorial current-carrying magnetodisk. The presence of a magnetodisk has been shown to influence the topology of a hot Jupiter's magnetosphere and to change a standoff distance of the magnetopause. In this paper, the basic features of the formation of a hot Jupiter's magnetodisk are studied by means of a laboratory experiment. A localized central source produces plasma that expands outward from the surface of the dipole and inflates the magnetic field. The observed structure of magnetic fields, electric currents, and plasma density indicates the formation of a relatively thin current disk extending beyond the Alfvénic point. At the edge of the current disk, an induced magnetic field was found to be several times larger than the field of the initial dipole.

Key words: methods: laboratory – planets and satellites: magnetic fields – planet–star interactions

1. INTRODUCTION

More than half of all known exoplanets have orbits around their host stars shorter than 0.6 AU. An evident maximum in the orbital distribution of exoplanets takes place in the vicinity of 0.05 AU. The majority of this population is represented by giant planets, or so-called hot Jupiters. Altogether, the hot Jupiters comprise about 30% of the total number of known exoplanets. Close location of a hot Jupiter to its host star results in intensive heating, ionization, and chemical modification of the planet's upper atmosphere by stellar X-ray/EUV (XUV) radiation. Expansion of the heated and ionized upper atmospheric gas leads to its continuous loss during interaction with the stellar wind (Lammer et al. 2003, 2007; Erkaev et al. 2005). A hot Jupiter's mass loss is closely linked to a set of general issues related to the evolution of planets, which has drawn considerable attention recently. One of these issues is the role of a hot Jupiter's magnetosphere in the protection of its ionosphere and upper atmosphere against the direct impact of stellar plasmas and energetic particles (e.g., cosmic rays; Khodachenko et al. 2007a, 2007b).

The magnetosphere of a close-in hot Jupiter is a complex object dependent on (a) stellar factors, e.g., stellar radiation, stellar wind plasma flow, and stellar magnetic field, and (b) planetary factors, e.g., orbital characteristics, escaping material outflow, and planetary magnetic field. Its morphology also depends on the speed of the stellar wind plasma relative to the planet (Erkaev et al. 2005; Ip et al. 2004). At sufficiently large orbital distances the stellar wind is supersonic and super-Alfvénic, and a Jupiter-type magnetosphere with a bow shock, magnetopause, and magnetotail is formed. The size of such a magnetosphere is characterized by the magnetopause standoff distance R_s, at which the balance between the stellar wind ram pressure and the pressure of the planetary magnetosphere field and escaping material is achieved. In cases of extremely close-orbit exoplanets (e.g., $d < 0.03$ AU for a Sun-like star), the stellar wind encountered is still accelerating and remains sub-magnetosonic and sub-Alfvénic (Ip et al. 2004; Preusse et al. 2005). Such exoplanets are expected to have Alfvénic-wing-type magnetospheres without shock (Ip et al. 2004).

For efficient protection of a planet possessing a Jupiter-type magnetosphere, the standoff distance R_s should be much larger than the height of the exobase (Grießmeier et al. 2004; Khodachenko et al. 2007b). Estimates show that an intrinsic magnetic dipole moment of a tidally locked close-orbit giant exoplanet alone is too weak to build a sufficiently large magnetosphere and protect the planetary upper atmosphere against non-thermal erosion by the stellar wind (Khodachenko et al. 2007a). To explain the survival of hot Jupiters in extreme conditions near their host stars, Khodachenko et al. (2012) proposed a more generic view of a hot Jupiter's magnetosphere. A key element in the proposed approach is to take into account the upper atmosphere of a planet as an expanding dynamical plasmasphere heated and ionized by the stellar XUV radiation (Johansson et al. 2009; Koskinen et al. 2010). Interaction of the outflowing plasma with the rotating planetary magnetic dipole field leads to the development of a current-carrying magnetodisk surrounding the exoplanet. The inner edge of the magnetodisk is located at the so-called Alfvénic surface ($r = R_A$), where the kinetic energy density of the moving plasma equals the energy density of the planetary magnetic field. This condition is also equivalent to the equality of the plasma ram pressure and magnetic pressure, or the Alfvén Mach number $M_A^2 = 1$. Beyond the Alfvénic surface, the expanding plasma is no longer guided by the dipole magnetic field. It deforms the field lines, leading to the creation of a current-carrying magnetodisk which in turn entirely changes the topology of the planetary middle and outer magnetosphere.

Two major regions with different topology of magnetic fields may be distinguished in the magnetosphere of a hot Jupiter driven by the escaping plasma flow (Mestel 1968). The first region corresponds to the inner magnetosphere, or so-called

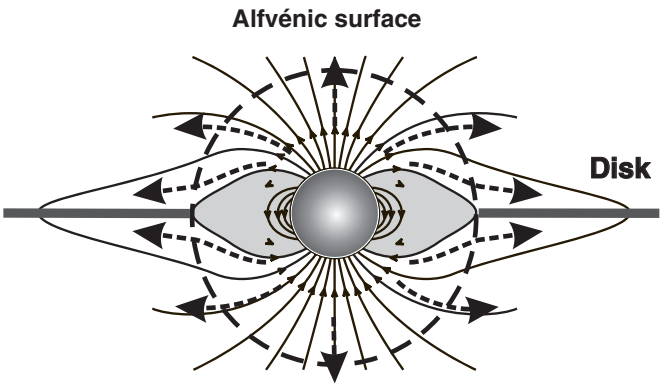

Figure 1. Schematic view of a magnetodisk formed by outflowing plasma in a dipole magnetic field beyond the Alfvénic surface (long-dashed line). The Shaded area indicates the dead zone region.

dead zone, filled with closed dipole-type magnetic field lines. The magnetic field in the dead zone is strong enough to keep plasma locked with the planet. In the second region, the so-called wind zone, the expanding plasma drags and opens the magnetic field lines. These two regions are separated by an Alfvénic surface $r = R_A$ (see Figure 1). The plasma escaping along field lines beyond the Alfvénic surface not only deforms and stretches the original planetary dipole field, but also creates a thin disk-type current sheet in the equatorial region (Figure 1). Altogether, this leads to the development of a new type of magnetodisk-dominated hot Jupiter magnetosphere, which has no counterpart among the solar system planets (Khodachenko et al. 2012). Understanding the specific features and possible observational manifestations of magnetospheres driven by the expanding planetary plasma flow appears to be a real aim of modern space physics.

Most of the existing studies on exoplanetary mass loss usually ignore issues related to the interaction of flow of escaping material with the planetary magnetic field (Lammer et al. 2003; Yelle 2004, 2006; Erkaev et al. 2005; Tian et al. 2005; Penz et al. 2008), and only a few attempts have been made to take this into account. For example, Trammell et al. (2011) studied the magnetosphere of a hot Jupiter by considering the specifics of plasma dynamics in the dead and wind zones. A global magnetic field was prescribed by an empirical model including an equatorial current sheet placed outside the dead zone. Thus, a question of self-consistent formation of the current-carrying equatorial magnetodisk remained out of the scope in Trammell et al. (2011).

According to Khodachenko et al. (2012), a hot Jupiter's magnetodisk can be formed by different mechanisms acting simultaneously: (1) the thermal expansion of the escaping planetary plasma envelope, heated by the stellar radiation, and (2) the centrifugal acceleration of plasma by rotating the planetary magnetic field in the co-rotation region, with subsequent release of material in the vicinity of the Alfvénic surface (the so-called sling mechanism). A self-consistent description of both of these mechanisms represents an important and complex physical problem. So far only qualitative insight into the origin and interconnection of the inner (dipole-dominated) and outer (magnetodisk-dominated) parts of a hot Jupiter's magnetosphere was suggested in Khodachenko et al. (2012).

The process of formation of an exoplanetary magnetodisk might be studied not only within the frame of simplified theoretical and more complex numerical models, but also by means of laboratory experiments. Laboratory simulation provides an independent research method and provides data that cannot be obtained by other means. The present paper reports on such work undertaken at the space plasma facility of the Institute of Laser Physics in Novosibirsk.

The goal of the reported experiment was to study the dynamical interaction of an expanding plasma flow with a background dipole magnetic field. This problem was considered theoretically by Mestel (1968) applied to stellar wind and by Adams (2011) and Trammell et al. (2011) applied to a hot Jupiter. In our study, primary attention was paid to the formation of a disk-type plasma-magnetic structure with an induced equatorial ring current and corresponding modification of the magnetic field topology. In previous theoretical studies, the magnetodisk-type topology was usually prescribed in a non-self-consistent way (Mestel 1968; Trammell et al. 2011), or the current-carrying disk was artificially introduced into the system, based on general physical arguments (Khodachenko et al. 2012). Therefore, an experimental check of the theoretical expectations and demonstration of a real magnetodisk formed under laboratory conditions is a major purpose of the present work. The distortion of a dipole-like magnetic field by plasma pressure or centrifugal force has been discussed in the context of planetary magnetospheres (Alexeev et al. 2003; Belenkaya et al. 2005; Russel et al. 2008; Johansson et al. 2009; Khodachenko et al. 2012), and has been considered in laboratory experiments (Lehnert et al. 1974; Slough 2001; Funaki et al. 2007). However, in all these studies, the problem of magnetodisk formation was either not addressed self-consistently or addressed without sufficient details.

For a clearer separation of various active factors influencing the formation of an exoplanetary magnetodisk, our experimental study was aimed at simulation (as a first step) of only the expansion of plasma, without the inclusion of rotation effects. This situation is relevant for a close-orbit hot Jupiter tidally locked to its host star so that the rotation angular velocity ω_p is equal to that of the planet orbital revolution and is relatively slow. In this case, the radial expansion of the hot planetary plasma will dominate the co-rotation effects in the inner magnetosphere and therefore will determine the formation of a magnetodisk. In general, the priority of either thermal expansion or centrifugal (rotational) acceleration mechanisms in the formation of a magnetodisk is defined by the mutual relation of the corresponding Alfvénic surface radii $R_A^{(\mathrm{esc})}$ and $R_A^{(\mathrm{cent})}$ for the thermal and centrifugal escape, respectively. Determined from the equality of the magnetic field energy density with the kinetic energy density of escaping or rotating plasma, they satisfy the following relation: $(\overline{R}_A^{(\mathrm{esc})}/\overline{R}_A^{(\mathrm{cent})})^3 = (\overline{R}_A^{(\mathrm{cent})}\overline{\omega}_p)/(V_{\mathrm{esc}}/V_{J0})$, where the bar symbols in the Alfvénic radii indicate that they are scaled in units of planet radius. The dimensionless planetary rotation frequency $\overline{\omega}_p$ is normalized to that of the solar system Jupiter, V_{esc} is the thermal escape velocity, and $V_{J0} = R_J\omega_J \approx 12\,\mathrm{km\,s^{-1}}$ is the linear rotation velocity at Jupiter's surface. According to the estimates made in Khodachenko et al. (2012) for a Jupiter-like planet orbiting a Sun-like star at different orbits, the dimensionless "centrifugal" Alfvénic radius $\overline{R}_A^{(\mathrm{cent})}$ may vary from 3 to 7, whereas $\overline{\omega}_p$ takes values from 0.03 up to 1. Therefore, for a typical thermal escape velocity V_{esc} comparable to or a few times higher than V_{J0} in most of cases, $R_A^{(\mathrm{esc})}$ remains smaller than $R_A^{(\mathrm{cent})}$. This means that escaping plasma starts to modify the background planetary magnetic dipole field closer to the planet compared to what happens due to rotation.

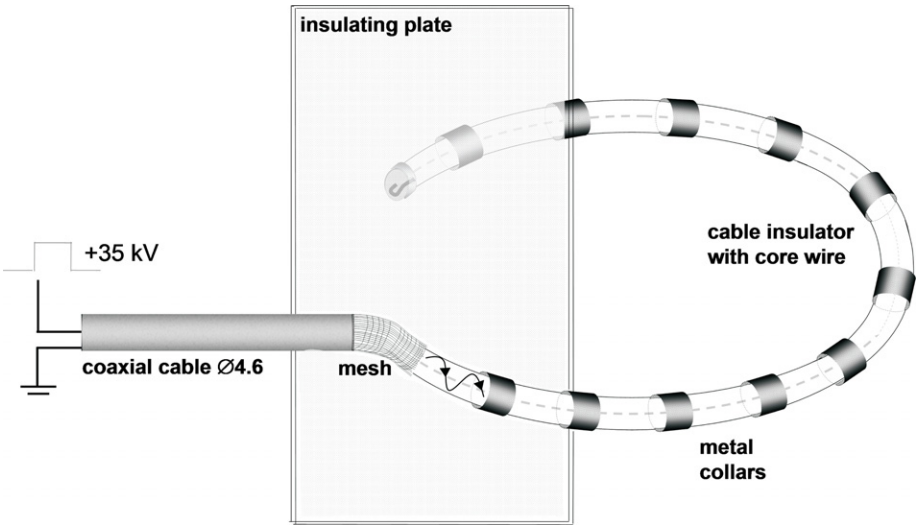

Figure 2. Plasma injector composed of a coaxial cable.

Interaction of low-beta plasma with a strong dipole field at such conditions, where the characteristic Alfvén surface size exceeds the available experimental volume, was studied in a number of previous experiments. In particular, in Lehnert et al. (1974), a stability of rotating plasma was investigated whereas Boxer et al. (2010) considered a confinement of turbulent plasma. The idea to increase the intensity and spatial extent of a magnetic dipole field by means of an expanding plasma flow was initially proposed in the context of a magnetoplasma sail (Winglee et al. 2000). The process was coined as dipole field inflation. To verify the technical feasibility of inflation, two laboratory experiments were conducted: one at Kyoto University and another at the University of Washington. In the first case (at Kyoto University), the plasma flow was generated by electric discharge in a gas jet, injected by a pulsed valve (Funaki et al. 2007). The magnetic moment, size of the dipole, and plasma velocity were approximately the same as in the experiment described in the present paper, though plasma density was somewhat lower. An increase of the magnetic field by a factor of two due to inflation from plasma was observed. In the second case (at the University of Washington), a helicon discharge was employed (Slough 2001). Because of the relatively low density of plasma, the additional magnetic field generated during this experiment constituted only a fraction of the initial dipole field. In that respect, we note that the results presented in this paper demonstrate stronger inflation, such that the generated magnetic field is several times larger than that of the background magnetic dipole in vacuum. This is mainly due to the plasma source used which generates denser and more energetic plasma but for a shorter time duration.

The paper is organized as follows. In Section 2, we provide a short description of the experimental setup and facility. In Section 3, the results of the interaction of the expanding plasma flow with the background magnetic dipole field are presented. Section 4 presents the numerical simulation of a case, similar to that realized in the laboratory experiment. In Section 5, we discuss the results we obtained and their relevance to hot Jupiters.

2. EXPERIMENTAL SETUP

Experiments have been carried out either in a large-scale KI-1 vacuum chamber with a size of Ø120 × 500 cm or in a smaller supplemental chamber with a size of Ø120 × 55 cm. For symmetric filling of the dipole magnetic field domain with plasma, injectors made of coaxial cable were used. The injector design is shown in Figure 2. The insulator containing a core wire is freed of the mesh and cable cover and then a series of cylinder collars made of metal foil are added. The collars' width and the gap between them is about 1 cm. The last collar is connected to the core wire. The cable with the collars is folded in a coil 9 cm in diameter. A dielectric plate is placed between the open mesh at the beginning of the cable and the open end of the core wire at the end of the cable to prevent discharge along the shortest path. When a pulsed voltage is applied to the core, the first gap between the mesh and the first collar breaks down along the surface of the insulator (as schematically shown in Figure 2). After that, the second gap breaks down and discharge propagates along the whole cable. Thus, plasma is generated by discharge along the dielectric surface in each gap between adjacent collars. For the given coil injectors the threshold of plasma production was approximately at 30 kV, and the voltage used in the experiments was 35 kV.

Two such injectors are attached to the cylindrical casing with radius, $R_D = 4.5$ cm. A pulsed magnetic dipole of size Ø5 × 5 cm and moment up to $M_D = 3 \times 10^5$ G cm^3 is placed inside the casing. According to the control measurements performed, the deviation of the spatial dependence of the real magnetic field from that for a pure dipole does not exceed 2% at distances $R > 10$ cm. A dipole-centered cylindrical coordinate system with Z-axis anti-parallel to the dipole moment is used in the paper. In this frame, injector coils were positioned above and below the equatorial plane at $z = \pm 2.8$ cm (see Figure 3). Magnetic field strength in this region reaches values up to 4 kG. Up to 10^{16} particles cm^{-2} of the cable surface are evaporated during the surface discharge and heated to temperatures from 10 up to a few tens of eV. After expanding to one diameter of the cable (~0.5 cm), this initial plasma has a thermal energy density about one order of magnitude smaller than the energy density of the background magnetic field. A typical condition for a hot Jupiter's upper atmosphere heated by EUV is when the thermal energy density of ionized atmospheric gas is much smaller than the magnetic field energy density. In that sense the dipole field in the experiment was strong enough to remain similar to the real planetary conditions. Diagnostics used in the

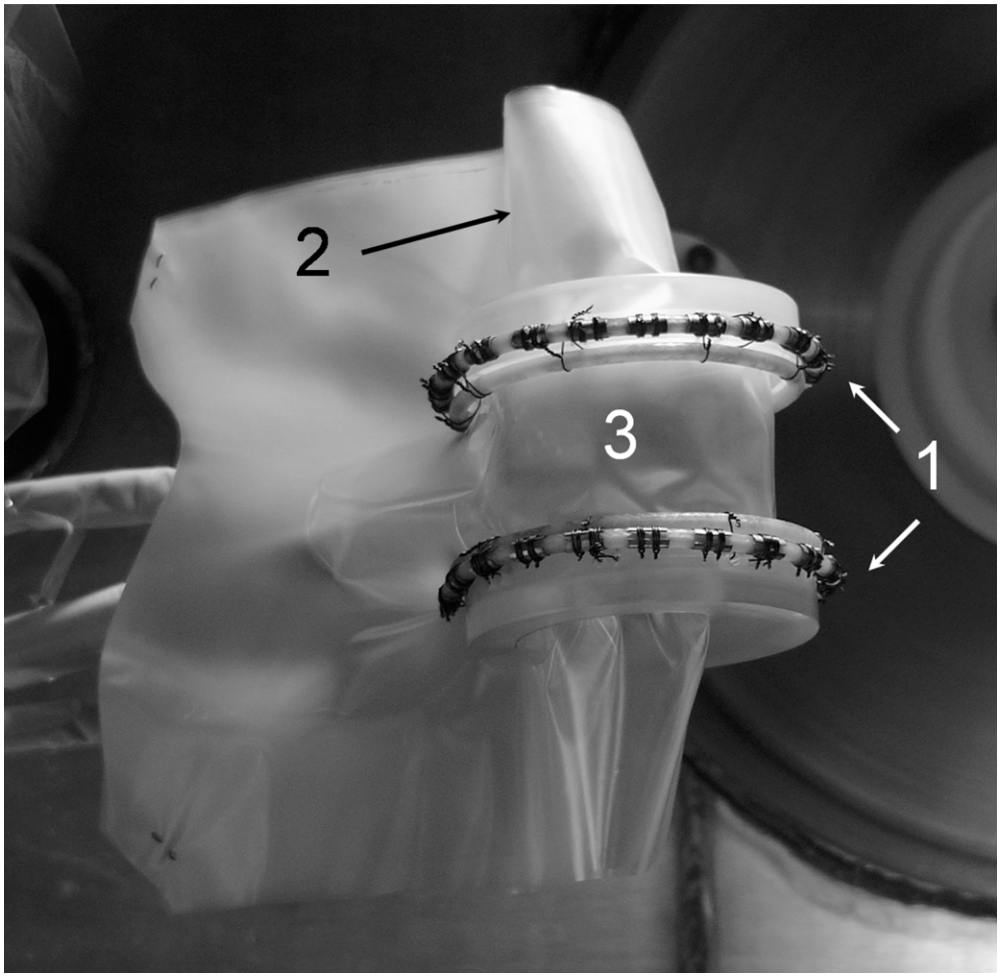

Figure 3. Experimental setup: coil injectors (1) with an insulator (2) covering the dipole casing (3).

experiment consisted of a Langmuire probe to measure charge density, a Faraday cap to measure ion flux density, a Rogovski coil to measure the current in plasma, and several magnetic probes. The probes were movable in the radial direction in the equatorial plane and across it up to a distance of ± 10 cm. Due to the pulsed mode of the discharge operation, each particular measurement in space was performed in a separate experimental run or shot.

3. RESULTS OF THE EXPERIMENT

3.1. Expanding Plasma Flow

An example of a typical measurement of plasma flux generated by coils is presented in Figure 4. The top panel gives the discharge current at the coils. It shows damped oscillations with a period of 4.5 μs caused by cable inductance and the storage capacitor. The next panels give the ion flux density $J_i = z_i e n_i V$ measured by a Faraday cup at two distances from the injectors. One can see that it is also modulated. It was found that each half-cycle of discharge current produces plasma. The corresponding sequential modulations of plasma flux density (marked by numerals) are clearly visible in Figure 4. After the second pulse, the plasma flow modulations overlap sufficiently well to constitute a continuous flux. At the time when the fourth half-cycle of discharge current starts to generate plasma, the plasma produced by the first half-cycle reaches a distance of about 40 cm which is much larger than the injector size.

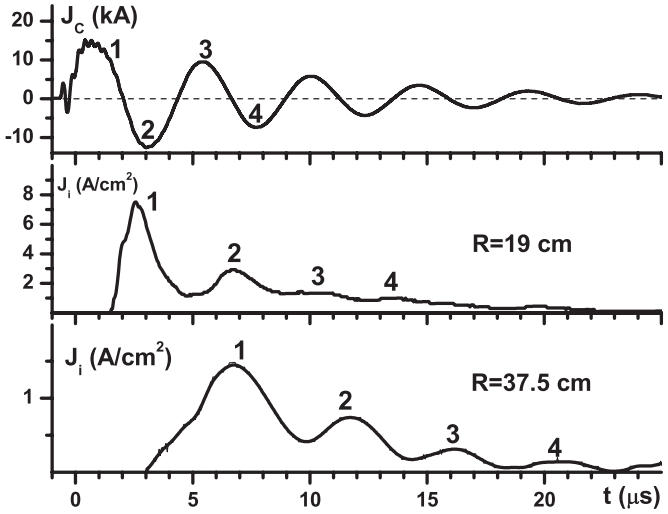

Figure 4. Dynamics of the discharge current in the coil injectors (top panel) and ion flux density measured by a Faraday cup at two distances (19 cm and 37.5 cm) from the dipole center.

The energy and number of ions produced decrease from cycle to cycle as the discharge current falls. The plasma generated by the first, second, and third half-cycles of electric current expands with velocity $V \approx 50, 40, 30\,\mathrm{km\,s^{-1}}$, respectively. This can be seen in the time-of-flight diagram in Figure 5.

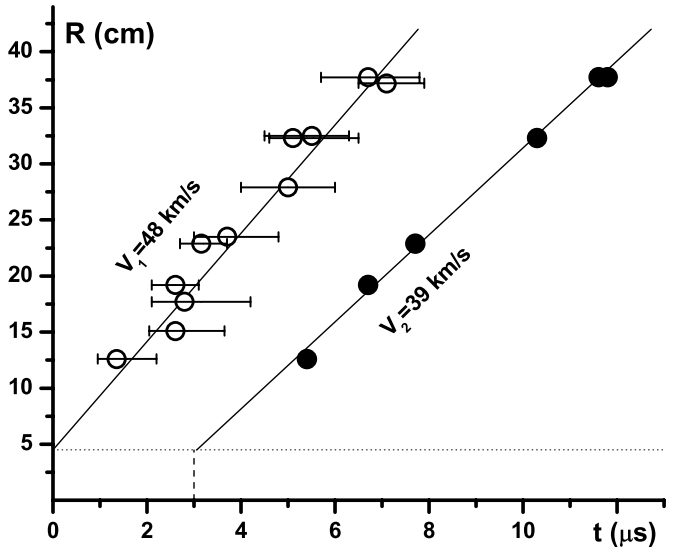

Figure 5. Time-of-flight diagram of the first (open circles) and second (full circles) maxima of plasma flow. Bars indicate positions at 75% of the maximum ion flux value. Straight lines show the mean square fit. Dashed lines mark the radial position of coil injectors and time of the second half-cycle maximum.

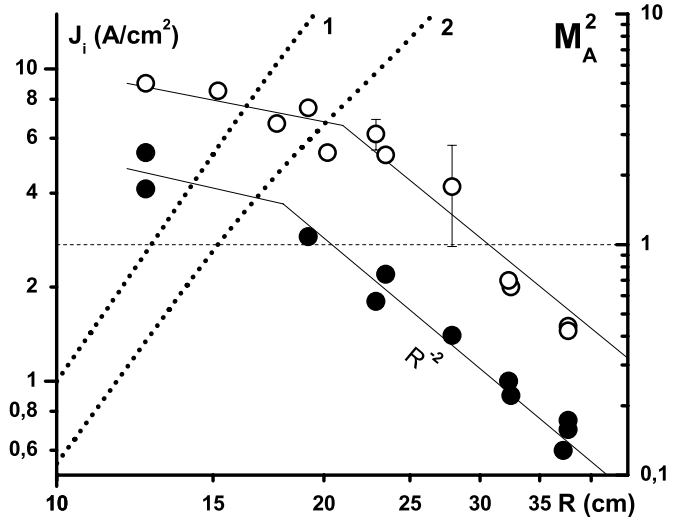

Figure 6. Dependence of ion flux on distance for the first (open circles) and second (full circles) maximum of plasma flow. Dotted curves show the calculated Alfvén-Mach number: (1) and (2) correspond to the first and second maxima.

The typical particle density stays in the range 10^{12}–10^{13} cm^{-3}. The amplitude of the ion flux density at large distances decreases approximately as $1/R^2$ (see Figure 6). This is to be expected for a quasi-stationary plasma source. Because of the finite source size, the spatial behavior of the ion flux density close to the dipole ($R < 15$ cm) is different from that in the far region.

The main parameters of the plasma flow can be derived from Figures 4–6. The ram pressure $p_k = n_i m_i V^2$ directly follows from the measured ion flux density and velocity as $p_k = (m_i/z_i e) \cdot J_i \cdot V$. It may be reasonably supposed that plasma consists of the same particles as a material of the discharge cable—two hydrogen ions for each carbon ion, which is singly ionized. In this case, the average ion mass is $\langle m_i \rangle = 14/3$, and the average charge is unity. The only parameter not measured is electron temperature. It rapidly falls during the outward expansion of plasma from the source due to conversion of the thermal energy into kinetic energy. Due to

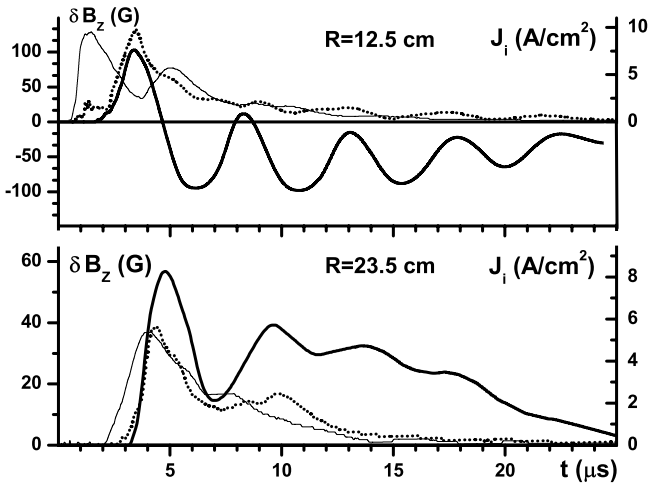

Figure 7. Dynamic of the main magnetic component perturbation δB_z (thick solid lines) measured in the equatorial plane close to the dipole (top panel, $R =$ 12.5 cm) and far from it (bottom panel, $R = 23.5$ cm). Dotted lines show the ion flux density under the same conditions; thin solid lines show the ion flux density measured without the dipole field.

three-body recombination, electrons are partially heated and T_e is expected to be about 5 eV or lower. Thus, the thermal pressure is much smaller than the ram pressure.

3.2. Interaction of Expanding Plasma with the Dipole Magnetic Field: Formation of the Magnetodisk

The interaction of expanding plasma with a dipole field is determined by the Alfvén–Mach number $M_A^2 = 4\pi n_i m_i V^2/B^2 = 4\pi p_k/B^2$ which also relates the ram pressure to the magnetic pressure. The results of the calculation of the Alfvén–Mach number for the first and the second maxima of plasma flow are shown in Figure 6 by dotted lines. In the first approximation, the total magnetic field is assumed to be close to a dipole field. The validity of such an assumption was confirmed experimentally up to distances $R \leqslant 20$ cm. One can see that the Alfvénic radius which corresponds to the critical value $M_A = 1$ is reached at a distance of about 15 cm. It might be expected that at $R < 15$ cm plasma will flow along the magnetic field lines while at $R > 15$ cm it will drag them.

Figure 7 shows a perturbation of magnetic field δB_z generated in the equatorial plane ($Z = 0$) during the interaction of plasma flow with the background magnetic dipole field. It was measured by the magnetic probes. The total field in the equatorial plane is calculated as a sum of the perturbation and the dipole field in vacuum $B_{tot}(Z = 0) = \delta B_z + B_D$. Close to the dipole (top panel) it reveals strong oscillations that are not produced by plasma, but are related to the discharge current in the coils. These oscillations are generated at the coils and are transported by plasma. The meaningful signal can be deduced as an average level. Note that far from the source (bottom panel) the oscillations are less prominent, and the result of interaction between the moving plasma and the dipole field is clearly visible. In particular, there is a strong disturbance produced by the first maximum of plasma flow, followed by a sufficiently long main phase of interaction that lasts from 10 μs up to 20 μs and is supported by the second, third, and fourth maxima. One can see that the magnetic variation changes its sign at the boarder between the close and far regions of the dipole. This indicates the presence of an electric current. It is co-directed with the current that generates the dipole field.

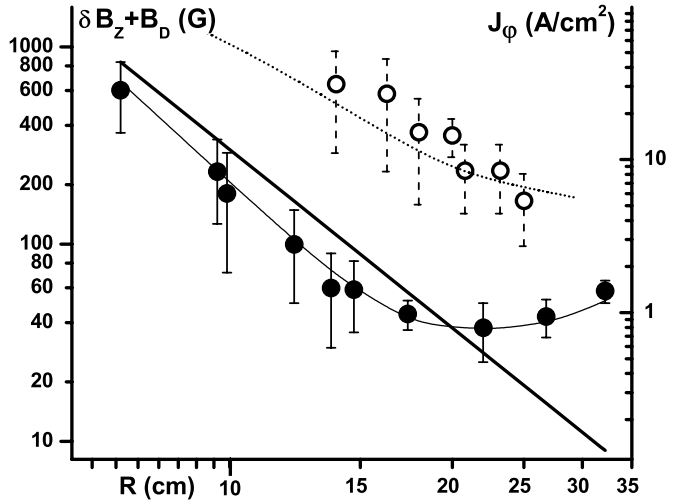

Figure 8. Left axis: the radial profile of the total magnetic field $\delta B_z + B_D$ (full circles) in the equatorial plane, $Z = 0$. The straight line shows the initial dipole field B_D. Right axis: current density in plasma obtained by a Rogovski coil (open circles) and calculated using magnetic measurements (dotted line).

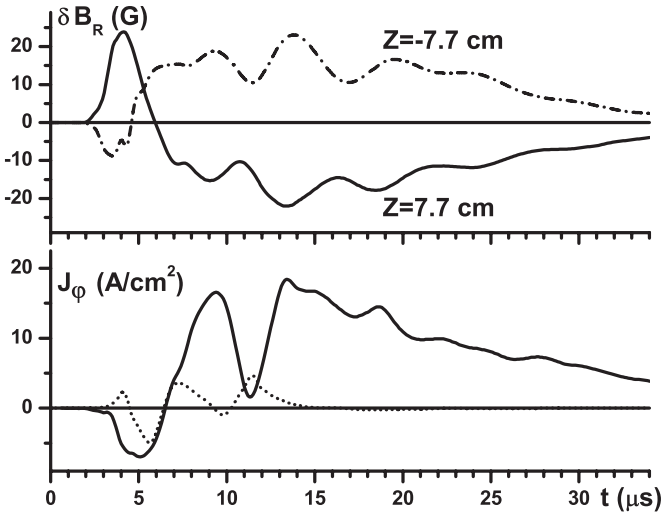

Figure 9. Top panel: dynamic of the radial component of the magnetic field perturbation δB_R measured above and below the equator at a radial distance of $R = 23$ cm. Bottom panel: current in plasma measured with Rogovski coil at a distance of $R = 20$ cm. Solid and dotted lines correspond to the measurements at the equator and at 12.5 cm above it, respectively.

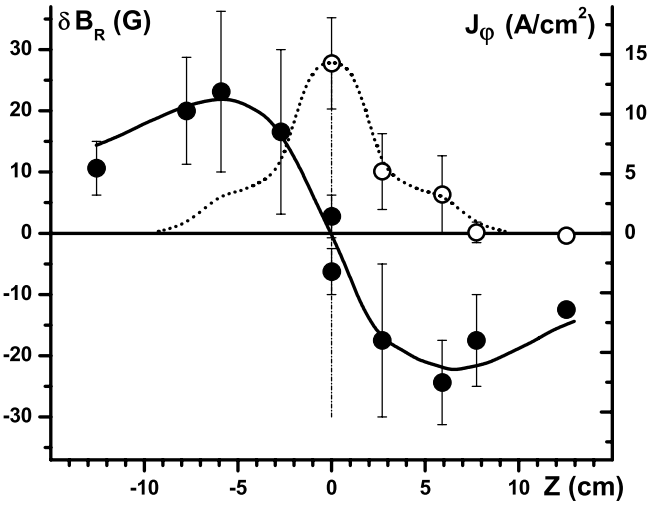

Figure 10. Profiles of the radial component δB_R (full circles, left axis) and current in plasma (open circles, right axis) across the equatorial plane at a distance of $R \approx 20$ cm.

Figure 7 also shows the ion flux density measured both in the presence of and without the background dipole field. At close distances, the magnetic field has an obvious influence on the motion of plasma. In particular, the first maximum of the ion flux is delayed by 2 μs when the dipole field is switched on (see the top panel). The delay can be seen at distances up to 20 cm. Beyond that, it becomes small as in the bottom panel of Figure 7. Such behavior indicates that, close to the dipole, plasma moves along the field lines, therefore the path from the injector to the probe is longer than a straight line.

The radial dependence of the total magnetic field in the equatorial plane ($Z = 0$) which is a sum of the variation δB_z generated by the induced electric current in plasma and the background magnetic dipole field is shown in Figure 8. For this plot, the measurements taken within the time interval 10–20 μs, which corresponds to the continuous phase of interaction supported by the second and third plasma flow maxima, were used. The error bars indicate maximum and minimum levels of the measured value caused by shot-to-shot variability as well as by the discharge modulations (as in the top panel of Figure 7). At least two shots per measurement have been made. One can see that at $R < 20$ cm the expanding plasma causes a decrease of the initial dipole field whereas at $R > 20$ cm the field is increased. Moreover, at $R > 25$ cm the resulting total field (including the generated one) is much larger than the initial dipole field and it is still increasing toward the end of the measurement region. At large distances (i.e., far from the disk location region) the additional current system creates a dipole-type magnetic field, however, near the disk, i.e., at the scale of the experiment, the additional field has a significantly non-dipole character. The magnitude of δB_zchanges monotonically from negative to positive values, and a change of magnetic flux in the measurement range is very small: $\delta\Phi = \int \delta B_z r dr \approx 0$. Estimation of a part of the current density associated with gradient of δB_z (about 120 G in 20 cm) yields $\approx$5 A cm^{-2}.

For direct measurement of the electric current in plasma, a Rogovski coil with a diameter of 4.6 cm was used. It was oriented along $\mathbf{e}_\varphi$ vector and it could be moved in the Z–R-plane. The radial profile of the measured current density J_φ is shown in Figure 8. Typical values are of the order of 10 A cm^{-2}.

A width of the magnetoplasma disk has been assessed by measuring the distribution along the Z-axis of the electric current and the perturbation of the radial component of magnetic field δB_R. The results of these measurements are presented in Figure 9. The top panel demonstrates that the spatial dependencies of δB_R above and below the equator are approximately anti-symmetric. The behavior of the azimuthal component of the electric current, J_φ, in plasma is shown in the bottom panel. After a couple of oscillations, J_φ stabilizes and then gradually decreases. A comparison of the measurements at $Z = 0$ and at $Z = 12.5$ cm reveals that the current is localized around the equatorial plane. Detailed profiles of J_φ and δB_R across the equatorial plane are presented in Figure 10. The radial magnetic field perturbation δB_R exhibits a typical reverse structure. The sign of perturbation corresponds to the stretching of the dipole field lines whereas its gradient ($\approx$35 G in 5.4 cm) gives a positive contribution of about 5 A cm^{-2} to the total electric current density. Note that the current detected with the Rogovski coil is confined within the width $\Delta Z \approx 12$ cm, which is consistent with

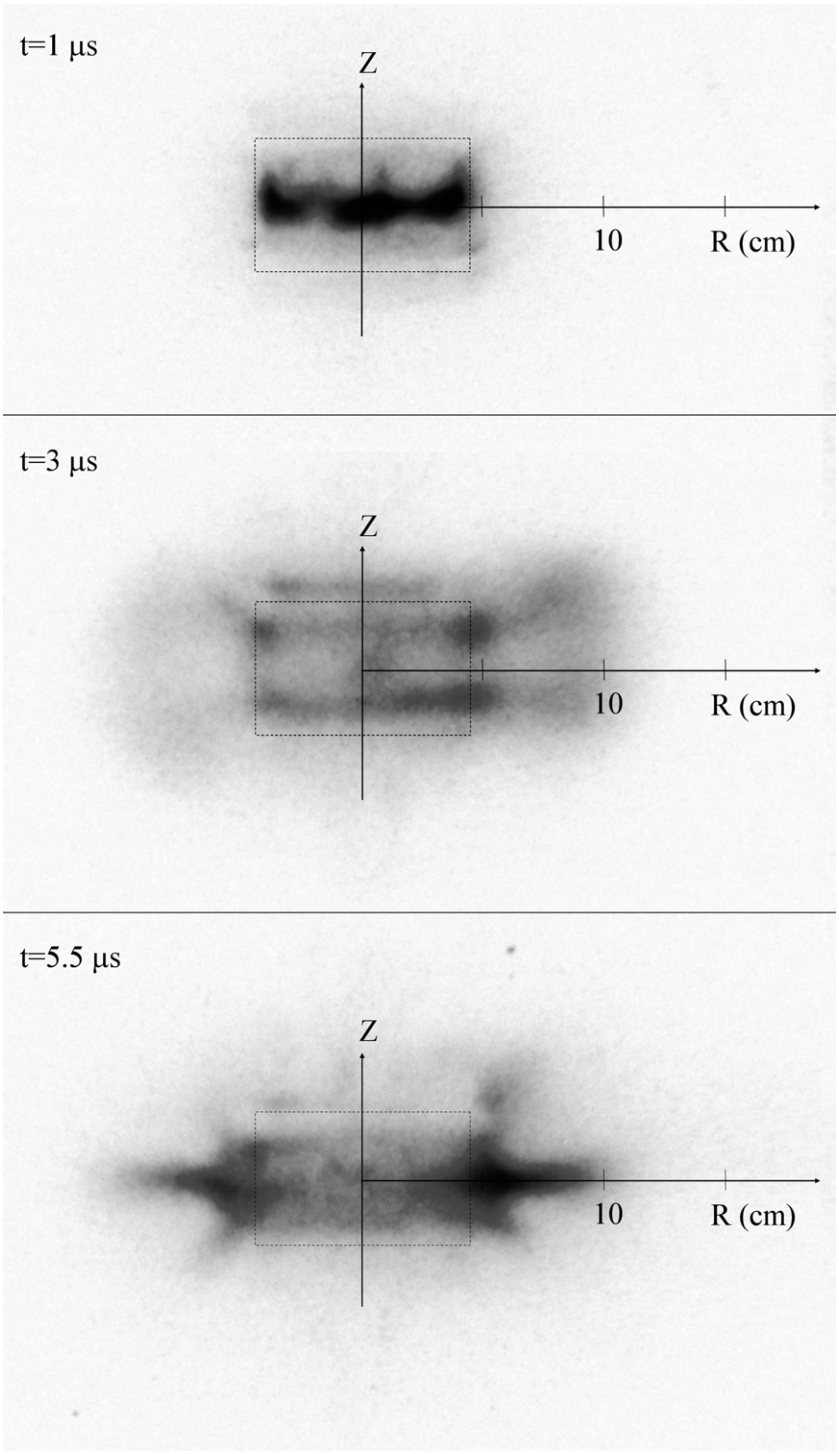

Figure 11. Short-time images of plasma expanding in a dipole magnetic field. Indicated moments of time correspond to the maximum of the first, second, and third half-cycles of discharge. The rectangle marks the dipole casing.

the measured $\delta B_{\rm R}$ profile. The most intensive electric current is concentrated in an even thinner layer $\Delta Z \approx 6$ cm.

At $R \approx 20$ cm the terms $\partial(\delta B_{\rm R})/\partial z$ and $\partial(\delta B_z)/\partial r$ are comparable to each other, but have an opposite sign. Note that for a dipole field these terms are of the same sign and also equal to each other. If we are to assume that this equality relation holds approximately true at all distances, then the current density can be estimated as $4\pi J_\varphi/{\rm c} = \partial B_z/\partial r - \partial B_{\rm R}/\partial z \approx 2\cdot\partial(\delta B_z)/\partial r$. The result of this calculation is shown in Figure 8 by the dotted line. Therefore, it can be seen that the two independent measurements give values that are in good general agreement.

Formation of a relatively thin equatorial disk was also observed in the snapshot plasma images (Figure 11) taken with an exposure of 30 ns. The first image was taken just after initiation of the discharge. In the second image, one can see a wide halo formed by plasma generated by the first half-cycle of discharge. The bottom image corresponds to the quasi-continuous phase of interaction when the plasma generated by the second and third half-cycles of discharge spans distances up

to 20 cm from the dipole. At this stage a thin equatorial disk appears. Because of the decrease of the plasma density with distance, only the inner part of the disk (e.g., up to $R \approx 15$ cm) is visible on the image. In fact, the disk extends much farther. It should be noted that without the dipole field no structure like this was seen except for spatial irregularities caused by the discharge.

The electric current generated due to inflation is affected by the Lorentz force which decelerates the radial expansion of plasma. Let us compare the initial kinetic energy of the plasma flow with the change of magnetic energy. The latter can be calculated only within the measurement range, i.e., for $14\,\mathrm{cm} \leqslant R \leqslant 25\,\mathrm{cm}$. Kinetic energy of plasma that comes into the interaction region can be calculated as a time-integrated flux $E_\mathrm{k} = 2\pi r^2 \int (n_\mathrm{i} m_\mathrm{i} V^2/2) \cdot V dt$ at a closest measured distance. The flux measured at the distance $R = 12.5$ cm (shown by the thin solid line in the top panel of Figure 7) is used for this calculation. The magnetic energy can be calculated as $E_\mathrm{b} = 2\pi \int (J_\varphi A_\varphi/2) \cdot r^2 dr$. In a zero-order approximation, the vector potential of an undisturbed magnetic dipole field $A_\varphi \approx M_\mathrm{D}/r^2$ may be taken. Finally, the calculations yield $E_\mathrm{k} \approx 0.5$ J and $E_\mathrm{b} \approx 0.26$ J. Therefore, the observed inflation of the magnetic field and current generation are consistent with the available energy of plasma flow. Next, we calculate an additional magnetic moment generated by the inflation: $M_\mathrm{add} = (4\pi/\mathrm{c})(1/2) \int (\mathbf{J} \times \mathbf{r}) \cdot d\upsilon = (4\pi/\mathrm{c}) 2\pi \cos\theta \int J_\varphi r^3 dr$. For the measured radial distribution of the electric current (Figure 8) and latitude angle 0.15 rad, derived from Figure 10, we obtain $M_\mathrm{add} \approx 7.5 \times 10^5$ G cm^3. This is 2.5 times larger than the initial dipole moment.

4. NUMERICAL SIMULATION

To assess the experimental results more comprehensively and to check their potential applicability for modeling of a hot Jupiter's magnetosphere, we performed a simple numerical simulation of the inflation process. An explicit 2D axisymmetric MHD code has been used on a rectangular mesh. A fixed pressure value and zero velocity conditions were specified at the surface of a hypothetical planet (the inner boundary of the simulation domain). A magnetic dipole was placed at the center of the planet. Gravity and rotation were set to zero to meet the conditions of the experiment. In such a case, there is only one characteristic parameter of the problem. It can be given as a ratio of sound and Alfvén speeds or as a plasma beta $C_S^2/V_A^2 = \beta_0$ at the inner boundary of the simulation box (the surface of the planet). Depending on this parameter, after the system is set into motion (i.e., plasma expansion takes place), another important characteristic may be established. This is the Alfvénic radius in the equatorial plane, i.e., the distance at which the density of the kinetic energy of the moving plasma becomes equal to the background magnetic field energy density, or in other words, where the ram pressure equals the magnetic pressure.

In the present paper, we consider just one particular case most relevant to the conditions realized in the laboratory experiment. More detailed numerical investigation of the system "magnetic dipole plus expanding plasma" and all its possible behavior regimes is a complex task which is beyond the scope of the present paper and deserves a separate publication with a full description of the numerical code and other details of the simulation.

In the experiment, the Alfvénic radius was estimated to be approximately 3 radii of the plasma source. This corresponds to plasma beta at the inner boundary of the simulation box $\beta_0 \approx 10^{-2}$. Figure 12 shows the distribution of electric current density, magnetic field lines, and plasma streamlines obtained in a numerical simulation with the same value of the inner boundary plasma beta as in the experiment. In full agreement with the experimental results and qualitative theoretical expectations (Mestel 1968; Trammell et al. 2011; Khodachenko et al. 2012), the magnetic field lines reveal open and closed regions. The region of closed field lines corresponds to the so-called dead zone of the stagnant plasma. In the open field line region plasma flows mostly along the field lines as it should in a stationary flow regime. The electric current color plot reveals the formation of an extremely thin and extended current sheet that begins immediately beyond the dead zone. This is also clearly seen from the reversible structure of the magnetic field compressed around the equatorial plane. Altogether, the structure obtained by this numerical simulation may be considered an idealized prototype of the current-carrying magnetodisk measured in our experiment.

Figure 12 also shows the relation between magnetic, ram, and thermal pressures as surfaces where $n_\mathrm{i} m_\mathrm{i} V^2 = B^2/8\pi$ and $2 n_i T = B^2/8\pi$. One can see that, as expected, close to the dead zone boundary, the magnetic force is balanced by thermal pressure. On the other hand, the ram pressure exceeds the magnetic pressure quite far from the dead zone, which may seem counterintuitive. However, this is a consequence of the magnetodisk presence due to which the magnetic field beyond the dead zone is significantly larger than the initial dipole field. Indeed, in comparison to the magnetic pressure of the initial dipole, the ram pressure becomes larger much closer to the dead zone boundary. Similar general relations are found to be true for the experimental data as well. At the farthest distance where the measurements have been made ($R \approx 32$ cm), the estimation of the ratio of ram to magnetic pressure for the undisturbed dipole field B_D and for the second plasma maximum yields $8\pi n_\mathrm{i} m_\mathrm{i} V^2/B_D^2 \approx 10$. However, for the total field B_tot it is smaller than unity $8\pi n_\mathrm{i} m_\mathrm{i} V^2/B_\mathrm{tot}^2 \approx 0.4$.

Note that in our MHD simulation the thickness of the magnetodisk is restricted only by mesh size whereas in reality (e.g., experiment), due to kinetic effects, it should not be much smaller than the ion gyroradius or ion inertia scale. Despite this limitation, the experiment and numerical MHD simulation show good general agreement, and confirm that an outward plasma expansion in the presence of a dipole field leads to the formation of a thin equatorial current sheet.

An important feature of the self-consistent magnetic field and electric current system of the magnetodisk, driven by the expanding plasma flow, consists of the presence of a continuous material flow. In that sense, an "equilibrium" state with a developed magnetodisk, achieved in the numerical simulations as well as similar configurations realized in the experiment and in the astrophysical objects, have essentially a dynamical character; static equilibrium (e.g., force balance) approaches are irrelevant for their description.

The results of both the numerical simulation and the experiment confirm the differentiation between the inner dipole-dominated region and the outer region controlled by the induced current system, which is a probable scenario for the structuring of magnetospheres of hot Jupiters (Khodachenko et al. 2012). Of special importance in that respect is the accumulation of plasma inside the dead zone within the Alfvénic surface and the formation of a magnetodisk in the equatorial plane of the dipole at distances beyond the Alfvénic radius. According to Khodachenko et al. (2012), these effects might play a crucial role

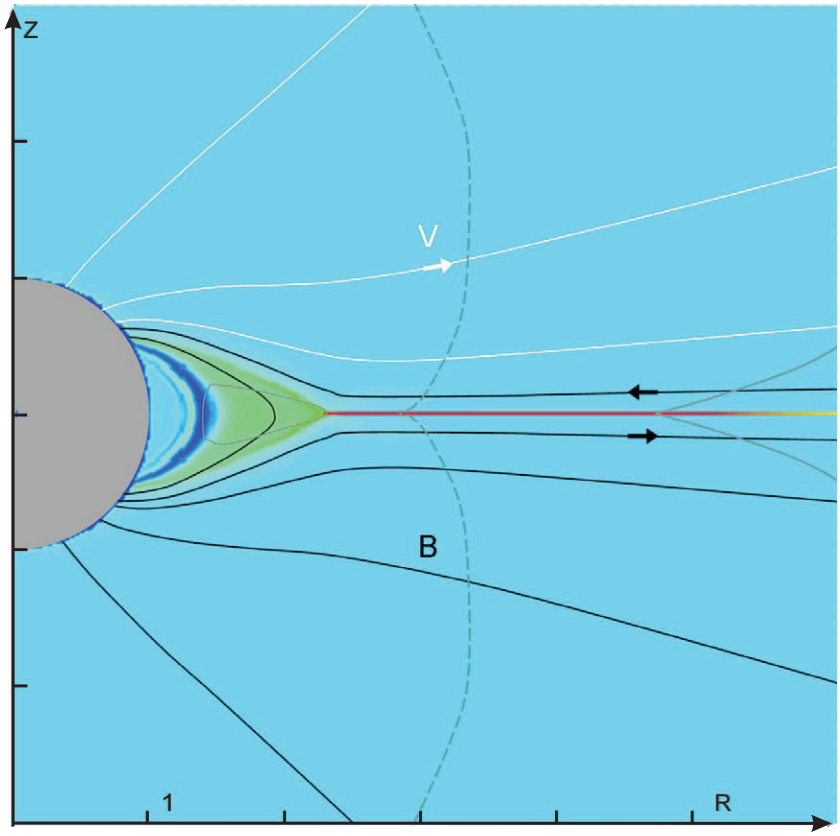

Figure 12. Electric current density J_φ obtained in the numerical simulation. Red (blue) color corresponds to a dimensionless value −2 (0.5). Magnetic field lines are shown in black and plasma streamlines in white. The solid gray line at the right side of the picture shows a surface where the plasma ram pressure equals the magnetic pressure. The same line close to the planet (in the dead zone) shows a surface where the thermal pressure equals the magnetic pressure. The dashed gray line in the middle of the image corresponds to the surface where the ram pressure equals the magnetic pressure of the initial dipole field.

in the scaling of magnetospheres of close-orbit hot Jupiters. Further experimental and theoretical investigations in that respect have to include a comparative study of the effects of rotation and interaction of an inflated magnetosphere with a stellar wind.

5. DISCUSSION AND CONCLUSIONS

The relevance of a modeling experiment to a natural phenomenon or a process is determined by dimensionless parameters. Limited, or physical, similarity is achieved when corresponding parameters are matched in a sense of being much smaller or much greater than unity (Podgornyi & Sagdeev 1970).

In the case of our experiment, the effects of planet gravity and rotation are absent. Thus, the results of the experiment can be applied to a plasma flow that is gravitationally unbound, for example, like stellar or comet wind. For a Jupiter-mass planet, this implies plasma with a temperature of the order of 10 eV. Rotation is important when the co-rotation velocity is larger than the plasma expansion velocity, or, as discussed in Section 1, when the "centrifugal" Alfvénic radius $R_A^{(\mathrm{cent})}$ becomes less than the Alfvénic radius $R_A^{(\mathrm{esc})}$ determined for the plasma expansion velocity. If we take an expansion velocity comparable to the escape velocity ∼50 km s^{-1}, the rotation becomes faster at a radial distance of about $4R_\mathrm{J}$ for the solar system Jupiter, but this distance remains significantly farther for close-orbit slowly rotating tidally locked exoplanets. As shown in Khodachenko et al. (2012), the value of $R_A^{(\mathrm{cent})}$ has a rather complicated dependence on different parameters of an exoplanet such as orbital distance, tidal locking, intrinsic planetary magnetic dipole moment, thermal mass-loss rate, etc. At the same time, in most cases of slowly rotating close-orbit hot Jupiters near solar-type stars, the value of $R_A^{(\mathrm{cent})}$ is ∼6–15 R_J (Khodachenko et al. 2012) which is several times larger than $R_A^{(\mathrm{esc})}$. Thus, the effects of thermal expansion and escape of planetary plasma are more important to the shaping of the magnetospheric field structure than the rotation.

Next, we consider plasma parameters. At the surface of a hot Jupiter the plasma thermal and kinetic betas are supposed to be very small. These conditions are fulfilled in the present experiment as demonstrated in Figure 6. Because the density of out-flowing plasma decreases as $\sim R^{-2}$ while the dipole magnetic field drops as $\sim R^{-3}$, a critical distance $R_\mathrm{A} \equiv R_A^{(\mathrm{esc})}$ exists at which the ram pressure of the plasma flow equals the magnetic pressure, or, in other words, the Alfvén Mach number is unity: $M_\mathrm{A}^2 = 1$. In the experiment, this condition is fulfilled at a distance $R_\mathrm{A} \approx 15\,\mathrm{cm} \approx 3\,R_\mathrm{D}$. For a Jupiter-sized planet ($R_\mathrm{p} = R_\mathrm{J}$) with a surface field of 1 G, the same relation ($R_\mathrm{A} = 3\,R_\mathrm{J}$) holds true if hot plasma with a particle energy of 10 eV has a density of about $10^8\,\mathrm{cm}^{-3}$ close to the planet's surface. The same estimate can be obtained based on a mass-loss rate of a planet instead of a surface density. Taking the mass-loss rate $\dot{M} = 10^{10}\,\mathrm{g\,s}^{-1}$, one gets $R_\mathrm{A}/R_J = 5$ and 7.5 for a plasma speed of 50 km s^{-1} and 10 km s^{-1}, respectively. These values seem to be consistent with the estimations obtained in other works (e.g., Khodachenko et al. 2012); however, in the case of a stronger planetary intrinsic magnetic field, the value of R_A/R_J becomes higher. A comparison of the major parameters is given in Table 1.

Table 1
Dimension and Dimensionless Parameters

Parameter	Experiment	Hot Jupiter
Planet radius, R_p (cm)	4.5	$\sim 10^{10}$
Magnetic moment ($A \cdot m^2$)	3×10^3	10^{26}–10^{27}
Temperature, T_e (eV)	~5	1–10
Plasma velocity V (km s^{-1})	30–50	$\geqslant 10$
Gravitational escape velocity (km s^{-1})	0	~50
Rotation velocity at R_p (km s^{-1})	0	1–10
Alfvénic radius, R_A/R_p	≈3	5–10
Interaction time, tV/R_A	≈6	$\gg 1$
Reynolds number, $4\pi\sigma R_A V/c^2$	~30	$\gg 1$
Hall parameter, $4\pi e n_e R_A V/cB$	1.5	$\gg 1$
Gyroradius, R_L/R_A	≈1	$\ll 1$

Finally, due to the relatively small scale of the laboratory experiment there are always considerations concerning kinetic effects. These are described by ion-inertia length and ion gyroradius. For planets they are negligibly smaller than the scales of interest. Taking the experimental parameters measured at a distance of 30 cm: field 50 G, velocity 40 km s^{-1}, and ion flux density 1 A cm^{-2}, one finds that kinetic scales are approximately equal to the same 30 cm. Thus, kinetic effects cannot be totally neglected (Moritaka et al. 2010). However, as previous experiments show (Ponomarenko et al. 2008), the MHD features of interaction which are of interest here remain basically the same.

The major purpose of the present laboratory study of the interaction of an expanding plasma flow with a background magnetic dipole field was to demonstrate experimentally the expected formation of a magnetodisk around a hot Jupiter and the related process of inflation of the initial planetary dipole magnetic field. In the case of expanding plasma envelopes of a hot Jupiter, these processes may lead to significant increase of the planetary magnetosphere size and contribute, therefore, to better magnetospheric protection of the planet against the impact of stellar wind and energetic particles. The experiment we conducted gives evidence of magnetodisk formation, supported by measurements of the magnetic field and current in plasma and short-time images. The inflated field, or the field generated by induced currents, sufficiently far from the dipole center, is much larger than the initial dipole field. The current system generated by outflowing plasma, as well as the plasma distribution around the source, has a typical disk structure. The observed aspect ratio is about $\Delta Z/R \leqslant 0.3$, and the disk width for given experimental parameters is comparable to or smaller than an ion gyroradius. If there is sufficient space around the dipole, the generated current adds to the overall magnetic moment of the system and this part might greatly exceed the initial dipole moment (several times in the present experiment). The magnetopause standoff distance is determined by the pressure of the total magnetospheric magnetic field. Thus, if, in the experiment case, the ram pressure of the external plasma wind does not exceed the pressure of the 50 G field, then, judging from Figure 8, the standoff distance should be at $R_s \approx 30$ cm with inflation, and only $R_s \approx 15$ cm otherwise. The estimations of magnetopause standoff distance R_s for a hot Jupiter from Khodachenko et al. (2012) give $R_s = (8\text{–}24)\,R_J$ and $R_s = (5\text{–}15)\,R_J$ for the cases with and without inclusion of a magnetodisk, respectively. Therefore, both experimental and theoretical studies predict the increase of planetary magnetosphere size by approximately double due to the presence of a magnetodisk.

Finally, it is also worth mentioning a certain physical analogy of a hot Jupiter's magnetodisk to some other astrophysical disks (Belenkaya & Khodachenko 2012) and space phenomena. In particular, it is similar to a heliospheric (astrospheric) current sheet formed under the conditions of the expanding solar (stellar) wind and a slowly rotating magnetic field of the Sun (star). The Jovian and Saturnian magnetodisks, in spite of their different origin mechanism, may also sometimes be referred to as analogous to a hot Jupiter's magnetodisk. Therefore, to a certain extent, the reported experiment and numerical simulation may be related to these astrophysical objects as well.

This work was supported by SB RAS Research Program grant II.8.1.4., RFBR grants 09-08-00970, 12-02-00367, and OFN RAS Research Program No. 22. M.L.K. acknowledges the projects P21197-N16, P25587-N27, and S11606-N16 of the Austrian Science Foundation (FWF). The authors are grateful for the EU FP7 projects Europlanet-RI/JRA3-EMDAF and IMPEx for partial support of experimental work as well as follow-up research communication and collaboration visits.

REFERENCES

Adams, F. C. 2011, ApJ, 730, 27
Alexeev, I. I., Belenkaya, E. S., Bobrovnikov, S. Yu., & Kalegaev, V. V. 2003, SSRv, 107, 7
Belenkaya, E. S., Bobrovnikov, S. Yu., Alexeev, I. I., Kalegaev, V. V., & Cowley, S. W. H. 2005, P&SS, 53, 863
Belenkaya, E. S., & Khodachenko, M. L. 2012, IJAA, 2, 81
Boxer, A. C., Bergmann, R., Ellsworth, J. L., et al. 2010, NatPh, 6, 207
Erkaev, N. V., Penz, T., Lammer, H., et al. 2005, ApJS, 157, 396
Funaki, I., Kimura, T., Ueno, K., et al. 2007, in Proc. 30th Int. Electric Propulsion Conf., Florence, IEPC-2007–94, http://erps.spacegrant.org/uploads/images/images/iepc_articledownload_1988–2007/2007index/IEPC-2007-094.pdf
Grießmeier, J.-M., Stadelmann, A., Penz, T., et al. 2004, A&A, 425, 753
Ip, W.-H., Kopp, A., & Hu, J.-H. 2004, ApJL, 602, L53
Johansson, E. P. G., Bagdonat, T., & Motschmann, U. 2009, A&A, 496, 869
Khodachenko, M. L., Alexeev, I. I., Belenkaya, E., et al. 2012, ApJ, 744, 70
Khodachenko, M. L., Lammer, H., Lichtenegger, H. I. M., et al. 2007a, P&SS, 55, 631
Khodachenko, M. L., Ribas, I., Lammer, H., et al. 2007b, AsBio, 7, 167
Koskinen, T. T., Yelle, R. V., Lavvas, P., & Lewis, N. K. 2010, ApJ, 723, 116
Lammer, H., Lichtenegger, H., Kulikov, Y. N., et al. 2007, AsBio, 7, 185
Lammer, H., Selsis, F., Ribas, I., et al. 2003, ApJL, 598, L121
Lehnert, B., Hellsten, T., & Raggi, R. 1974, PhyS, 9, 53
Mestel, L. 1968, MNRAS, 138, 359
Moritaka, T., Usui, H., Nunami, M., et al. 2010, ITPS, 38, 2219
Penz, T., Erkaev, N. V., Kulikov, Y. N., et al. 2008, P&SS, 56, 1260
Podgornyi, I. M., & Sagdeev, R. Z. 1970, SvPhU, 12, 445
Ponomarenko, A. G., Zakharov, Yu. P., Antonov, V. M., et al. 2008, PPCF, 50, 074015
Preusse, S., Kopp, A., Büchner, J., & Motschmann, U. 2005, A&A, 434, 1191
Russell, C. T., Khurana, K. K., Arridge, C. S., & Dougherty, M. K. 2008, AdSpR, 41, 1310
Slough, J. 2001, in Proc. 27th Int. Electric Propulsion Conf., Pasadena, CA, IEPC-01-202, http://www.ess.washington.edu/space/M2P2/iepc.slough.PDF
Tian, F., Toon, O. B., Pavlov, A. A., & De Sterck, H. 2005, ApJ, 621, 1049
Trammell, G. B., Arras, P., & Li, Z.-Y. 2011, ApJ, 728, 152
Winglee, R. M., Slough, J., Ziemba, T., & Goodson, A. 2000, JGR, 105, 21067
Yelle, R. V. 2004, Icar, 170, 167
Yelle, R. V. 2006, Icar, 183, 508